

Magnetic phases of the quasi-two-dimensional compounds $\text{Fe}_x\text{Co}_{1-x}\text{Ta}_2\text{O}_6$

This article has been downloaded from IOPscience. Please scroll down to see the full text article.

2010 J. Phys.: Condens. Matter 22 496004

(<http://iopscience.iop.org/0953-8984/22/49/496004>)

View [the table of contents for this issue](#), or go to the [journal homepage](#) for more

Download details:

IP Address: 143.54.199.3

The article was downloaded on 01/12/2010 at 12:39

Please note that [terms and conditions apply](#).

Magnetic phases of the quasi-two-dimensional compounds $\text{Fe}_x\text{Co}_{1-x}\text{Ta}_2\text{O}_6$

E G Santos¹, S R de Oliveira Neto², E J Kinast³, J B M da Cunha¹, O Isnard⁴ and M A Gusmão¹

¹ Instituto de Física, Universidade Federal do Rio Grande do Sul, CP 15051, 91501-970 Porto Alegre, Brazil

² Universidade Federal de Sergipe, 49100-000 São Cristóvão, SE, Brazil

³ Universidade Estadual do Rio Grande do Sul, Rua Inconfidentes 395, 93340-140 Novo Hamburgo, Brazil

⁴ Institut Néel (CNRS) and Université Joseph Fourier, BP 166, 38042 Grenoble Cedex 9, France

Received 30 July 2010, in final form 8 October 2010

Published 23 November 2010

Online at stacks.iop.org/JPhysCM/22/496004

Abstract

We report new results on the magnetic properties of the $\text{Fe}_x\text{Co}_{1-x}\text{Ta}_2\text{O}_6$ series of compounds. Essentially using neutron-diffraction and magnetic measurements we study, in more detail, the low- x limit of the temperature versus x phase diagram, where a new bicritical point is observed. The complete phase diagram shows three different magnetic phases at low temperature, for a high, intermediate and very low iron content. These phases consist of distinct antiferromagnetic orderings, characterized by different pairs of propagation vectors. We obtain information about the intraplane exchange interactions by fitting a high-temperature series of the magnetic susceptibility. Here we improve on a previously employed model, showing that two non-equivalent next-nearest-neighbor interactions must be taken into account in order to allow for in-plane magnetic orderings that are consistent with the neutron-diffraction results.

1. Introduction

The ATa_2O_6 trirutile compounds with $A = \text{Co}, \text{Ni}$ or Fe present a rich variety of magnetic phases, dominated by low-dimensionality effects. Since the original investigation of the magnetic properties of FeTa_2O_6 by Eicher *et al* [1], many studies have followed, not only using magnetic measurements [2] but also Mössbauer spectroscopy [3], and elastic as well as inelastic neutron scattering techniques on powder or single-crystal samples [4, 5]. The magnetic ordering in Co and Ni isotope compounds has also been the subject of complementary investigations [6–10]. Recently, the CoTa_2O_6 compound has been reported to exhibit a different magnetic structure [11] than the one previously suggested [8]. In addition to its interesting magnetic properties, NiTa_2O_6 has also been found to be an interesting candidate for applications as a water-splitting photocatalyst [12]. Bicriticality has been discovered [13] in the $\text{Fe}_x\text{Co}_{1-x}\text{Ta}_2\text{O}_6$ series for $x = 0.46$, showing another interesting property of these compounds. Studies of magnetic properties have also been reported on $\text{Fe}_x\text{Ni}_{1-x}\text{Ta}_2\text{O}_6$ compounds [14, 15].

At this point it is worth summarizing the main features of the $\text{Fe}_x\text{Co}_{1-x}\text{Ta}_2\text{O}_6$ compounds. The entire series crystallizes in the trirutile structure, which is tetragonal with the $P4_2/mnm$ space group [16]. In such a structure, Fe^{2+} or Co^{2+} cations are located at the corners and center of each unit cell, i.e., at positions $(0, 0, 0)$ and $(1/2, 1/2, 1/2)$. These cation layers are separated by two layers of Ta^{5+} , at positions $z \sim 1/6$ and $z' \sim 1/3$ measured along the c direction. Each cation is surrounded by O^{2-} anions occupying the vertexes of an octahedron. The oxygen octahedra are distorted, having a shorter principal axis lying on the ab plane, and rotating by 90° upon a translation of $(1/2, 1/2, 1/2)$. These materials exhibit quasi-two-dimensional magnetic characteristics. They are paramagnetic at room temperature, present a broad maximum of the magnetic susceptibility near 15 K (a signature of short-range magnetic correlations), and order antiferromagnetically, with Néel temperatures between 5 and 9.5 K. FeTa_2O_6 presents a magnetic structure described by two propagation vectors, $(1/2, 0, 1/2)$ and $(0, 1/2, 1/2)$ [1], associated to magnetic ions at the corner and center of the structural unit cell, whose

magnetic moments are oriented perpendicularly to one another. In the following we will refer to this structure as AFF (F for Fe). On the other hand, CoTa_2O_6 presents a magnetic structure indexed by the propagation vectors $(\pm 1/4, 1/4, 1/4)$ [11], which we will call AFC (C for Co). A previous study of the $\text{Fe}_x\text{Co}_{1-x}\text{Ta}_2\text{O}_6$ series [13] showed that the magnetic ordering observed for FeTa_2O_6 is stable for high x values, from 1.0 down to 0.46, while the magnetic structure of CoTa_2O_6 is no longer present for iron concentrations as low as 9%, where a third phase appears that remains stable up to $x \sim 0.46$. This phase is described by the propagation vectors $(\pm 1/4, 1/4, 0)$, and will be called AFI (I for intermediate).

An important point concerning the magnetic phases revealed by neutron diffraction in $\text{Fe}_x\text{Co}_{1-x}\text{Ta}_2\text{O}_6$ compounds is that they imply the existence of strong magnetic (crystal-field) anisotropy. All magnetic moments lie on the ab plane, alternating along the directions $[1, 1, 0]$ and $[1, \bar{1}, 0]$ from one plane to the next, these easy-axis directions coinciding with the orientation of a shortened principal axis of the oxygen octahedron surrounding each magnetic ion. This 90° rotation of the moments from one magnetic plane to the next follows the corresponding rotation of the octahedra in the trirutile structure. Both the low-dimensional character and the strong in-plane easy-axis anisotropy are very robust features of these compounds. In fact, they are also evident in the paramagnetic phase where the susceptibility data can be fitted to a high-temperature series evaluated for a two-dimensional (2D) Heisenberg model with an in-plane easy axis and competing nearest-neighbor (nn) and next-nearest-neighbor (nnn) exchange interactions [2, 13].

Despite the large amount of information partially summarized above, gaps still exist in our understanding of the magnetism in the (Fe, Co) Ta_2O_6 series. In this paper, we will concentrate on two aspects. First, we will experimentally investigate the stability region of the AFC magnetic phase, and its coexistence with the AFI phase for samples with very low iron content. Second, we will revisit the 2D model employed for the paramagnetic susceptibility, which, as we will show, needs to be reformulated in order to yield values of exchange interactions that are consistent with the observed in-plane magnetic structures at low temperature.

2. Magnetic phases for low iron content

In order to determine more precisely the composition limit between the AFC and AFI magnetic phases, we prepared new powder samples of $\text{Fe}_x\text{Co}_{1-x}\text{Ta}_2\text{O}_6$, with $x = 0.01, 0.02$, and 0.04 . The samples were prepared as previously described [16]. The sample purity was first checked by x-ray diffraction (XRD) analysis before carrying out magnetic measurements and neutron-diffraction experiments. The XRD analysis was performed with a Siemens D500 diffractometer, in Bragg-Brentano geometry, using $\text{Cu K}\alpha$ radiation, $\lambda(\text{K}\alpha_1) = 1.54056 \text{ \AA}$ and $\lambda(\text{K}\alpha_2) = 1.54439 \text{ \AA}$, with a scan step of 0.02° and an angular 2θ range from 10° to 120° . The structure parameters were confirmed to be in agreement with those previously obtained for the whole series [13].

2.1. Magnetic measurements

The magnetic measurements were carried out using an extraction magnetometer, in a wide temperature range, from 1.5 to 300 K. Both the isothermal magnetization, $M(H)$, and the temperature-dependent susceptibility, $\chi(T)$, were measured. The $M(H)$ curves were recorded in a magnetic field ranging from 0 to 100 kOe. $\chi(T)$ was obtained by field-cooling the samples at a constant magnetic field of 5 kOe, then keeping the field fixed and measuring the magnetization while raising the temperature. Above 50 K, for better accuracy, the values of magnetic susceptibility were extracted from ‘Arrot plots’ of the isothermal magnetization. In other words, $1/\chi(T)$ was obtained by extrapolating the linear part of H/M versus M^2 curve down to $M = 0$ [17].

The samples order with an antiferromagnetic structure at low temperatures. We achieved a precise determination of the Néel temperature T_N by measuring the susceptibility at intervals of 0.2 K in the range from 1.5 to 20 K, and numerically performing the derivative $\partial(T\chi(T))/\partial T$, which presents a well defined peak at the transition. The Néel temperature showed a marked reduction from $x = 0$ to 0.01, and then started to rise again towards the value previously obtained [13] for $x = 0.09$. This is similar to what was observed near $x = 0.46$ [13], and can be interpreted as another bicritical point in the T versus x phase diagram. This interpretation is corroborated by neutron-diffraction experiments, as discussed below.

2.2. Neutron diffraction

Neutron-diffraction data were collected with a double-axis, multicounter, high-flux diffractometer (D1B) at the Institute Laue Langevin (ILL), in Grenoble, France, using a wavelength of 2.52 \AA selected by a pyrolytic graphite monochromator. In the configuration employed, the D1B resolution was about 0.3° (fwhm), and the multicounter was composed of 400 cells covering a total angular (2θ) range of 80° , from 5° to 85° , with a detector step of 0.2° . The 2θ range was checked down to 2° , enabling us to rule out the possible occurrence of other magnetic Bragg reflections.

We analyzed our neutron-diffraction data using the FULLPROF refinement package [18] in order to extract crystallographic and magnetic parameters. The agreement factors used in this work are defined according to the guidelines of the Rietveld refinement [19]. The neutron scattering lengths used were $0.5803 \times 10^{-12} \text{ cm}$ for Ta, $0.9450 \times 10^{-12} \text{ cm}$ for Fe, $0.2490 \times 10^{-12} \text{ cm}$ for Co, and $0.5803 \times 10^{-12} \text{ cm}$ for O; the values were taken from Sears [20].

Figure 1 shows the neutron spectra for three samples in the limit of very low iron concentration: $x = 0, 0.01$, and 0.02 . We have cut off the intensity scale in order to make the magnetic reflections more visible. The first sample, which is just CoTa_2O_6 , is indexed by the propagation vectors of the AFC structure, i.e., $(\pm 1/4, 1/4, 1/4)$. The last one is already completely indexed by the propagation vectors corresponding to the AFI structure, $(\pm 1/4, 1/4, 0)$. For the sample with $x = 0.01$ we observe the presence of both kinds of reflection, indicating the coexistence of these two

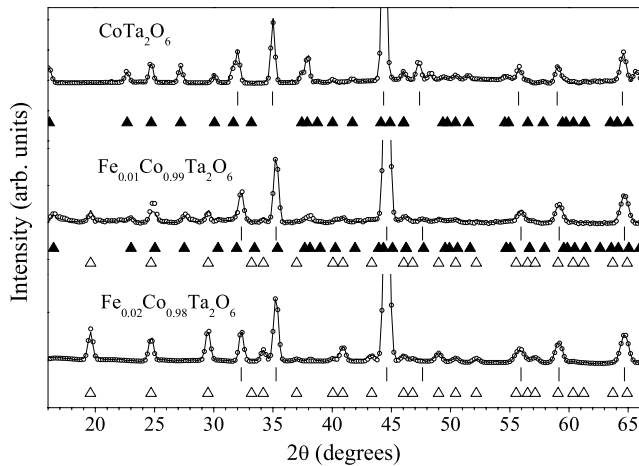


Figure 1. Neutron-diffraction spectra showing phase coexistence at $x = 0.01$ for the $\text{Fe}_x\text{Co}_{1-x}\text{Ta}_2\text{O}_6$ solid solution. The reflections indicated by solid triangles correspond to the magnetic phase described by propagation vectors $(\pm 1/4, 1/4, 1/4)$, while open triangles mark reflections of the phase with propagation vectors $(\pm 1/4, 1/4, 0)$. The vertical bars locate structural reflections of the $P4_2/mmm$ space group. The continuous lines are Rietveld fittings to the data points.

magnetic phases. A similar coexistence pattern was observed earlier for concentrations near $x = 0.46$ [13], in this case involving the AFI and AFF phases. The above result confirms that a bicritical point exists at $x \simeq 0.01$ in the T versus x phase diagram. It is worth mentioning that the Rietveld fitting of magnetic reflections is poorer for the sample with phase coexistence, as can be seen in figure 1. Even though the peaks are clearly present, they appear somewhat smeared out or slightly distorted. We believe that this is due to the existence of magnetic frustration, so that parts of the sample might not develop long-range magnetic ordering. The main point is that we have two different coexisting magnetic structures, and the change from one to the other is induced by the Fe content. One can suppose that there must be regions in which the Fe concentration is enough to suppress the AFC ordering, but not enough to stabilize the AFI phase.

2.3. Phase diagram

Putting together the information about the Néel temperature, obtained from susceptibility measurements, and about the ordered magnetic phases, obtained from neutron diffraction, we can complement the magnetic phase diagram of the $\text{Fe}_x\text{Co}_{1-x}\text{Ta}_2\text{O}_6$ solid solution, first appearing in [13]. The complete diagram, with two bicritical points, near $x = 0.01$ and $x = 0.46$, is shown in the top panel of figure 2. At various temperatures along the two vertical dotted lines neutron-diffraction experiments revealed the coexistence of the two phases that are stable on each side. This T versus x phase diagram correlates well with the variation of low-temperature magnetic moments with composition, as obtained from neutron-diffraction data, which can be seen in the bottom panel of figure 2. It is noticeable that there is a dramatic reduction of the magnetic moment for the two compositions

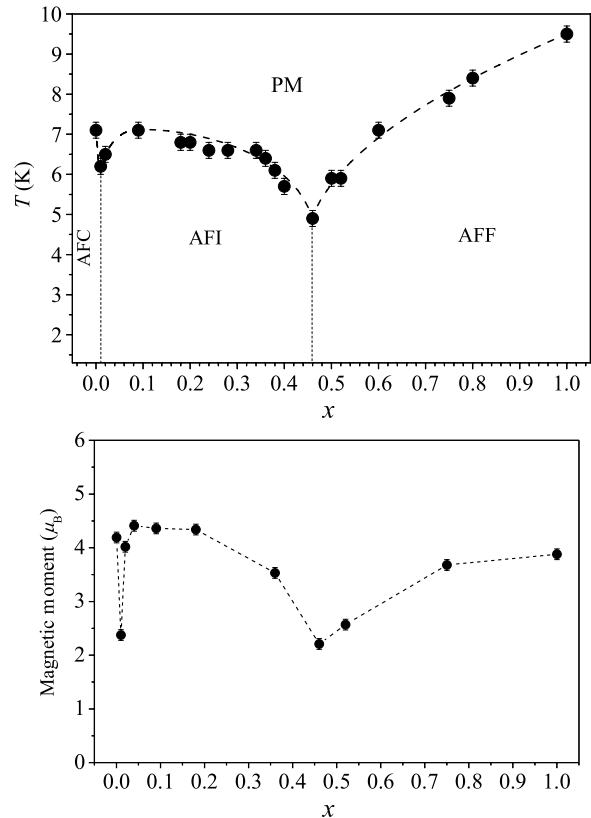


Figure 2. Top: T versus x phase diagram of the $\text{Fe}_x\text{Co}_{1-x}\text{Ta}_2\text{O}_6$ series. The solid circles are values of T_N obtained from magnetic-susceptibility measurements. The broken lines are guides to the eye. PM stands for the paramagnetic phase, while the ordered phases are labeled as defined in the text. Bottom: variation of the low-temperature magnetic moment as a function of concentration along the $\text{Fe}_x\text{Co}_{1-x}\text{Ta}_2\text{O}_6$ solid series, as deduced from refinement of neutron-diffraction data.

exhibiting coexistence of the magnetic phases, $x = 0.46$ and 0.01 . An average Fe/Co magnetic moment of only 2.2 and $2.5 \mu_B/\text{atom}$ is obtained for $x = 0.46$ and 0.01 , respectively. This is to be compared with $3.8 \mu_B$ for FeTa_2O_6 and about $4 \mu_B$ in CoTa_2O_6 [10, 11]. The origin of this reduction is probably the same as that mentioned in connection with the neutron-diffraction fittings of figure 1. The values of the magnetic moments are estimated from peak intensities assuming that the whole sample is magnetized in one or other of the two phases. Thus, the existence of a sizable fraction of the sample without long-range magnetic ordering certainly reduces the observed intensities, and hence the apparent local moment estimated from them.

3. Two-dimensional model revisited

Our previous discussion makes it clear that the $\text{Fe}_x\text{Co}_{1-x}\text{Ta}_2\text{O}_6$ compounds present three-dimensional AF ordering at low temperatures. Nevertheless, their crystal structure, low values of T_N , and overall shape of the magnetic susceptibility [13] provide strong evidence of quasi-two-dimensional characteristics. Thus, it is reasonable to expect that a purely two-dimensional model would be sufficient to describe their

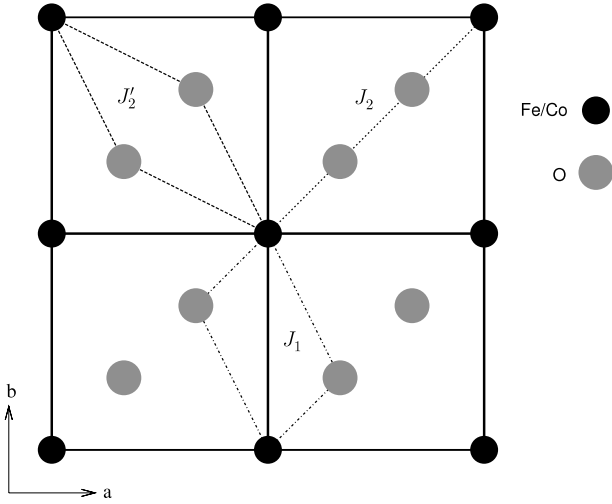


Figure 3. Superexchange paths between nearest and next-nearest neighbors on a magnetic ab plane (adapted from [5]).

high-temperature behavior. Such a model must take into account the observed strong crystal-field anisotropy, and include competing exchange interactions, since the in-plane magnetic ordering is not a Néel state.

The first model to show some success in interpreting the susceptibility behavior in FeTa_2O_6 was a two-dimensional anisotropic Heisenberg model proposed by Muraoka *et al* [2]. It involves nearest-neighbor (nn) and next-nearest-neighbor (nnn) exchange interactions, and is defined by the Hamiltonian

$$\mathcal{H} = -2J_1 \sum_{\langle ij \rangle}^{\text{nn}} \mathbf{S}_i \cdot \mathbf{S}_j - 2J_2 \sum_{\langle ij \rangle}^{\text{nnn}} \mathbf{S}_i \cdot \mathbf{S}_j - D \sum_i S_{iz}^2 - \mu_B \sum_i (g_{\parallel} H_z S_{iz} + g_{\perp} H_x S_{ix}). \quad (1)$$

The first two terms describe exchange interactions between spins \mathbf{S}_i and \mathbf{S}_j occupying, respectively, nn and nnn lattice sites, J_1 and J_2 being the corresponding exchange constants. A single J_2 was used in [2] despite the existence of two non-equivalent exchange paths, sketched in figure 3 (labeled by J_2 and J_2'), as pointed out by Hague *et al* [5]. In the third term, where D measures the anisotropy strength, the

easy axis z (in spite of this notation) lies on the ab plane, along the direction $[1, 1, 0]$ or $[1, \bar{1}, 0]$, as discussed before. The last term accounts for the effect of an applied magnetic field, with anisotropic g -factor.

Thanks to our knowledge about the magnetically ordered structures, obtained through neutron diffraction as described in the previous sections, we can check whether the observed spin configurations are consistent with that model. Even though the model is strictly two-dimensional, while the observed magnetic phases are also ordered along the c axis, we should expect in-plane interactions to be dominant in determining the spin configurations on the ab plane.

Two in-plane spin structures appear in the $(\text{Fe, Co})\text{Ta}_2\text{O}_6$ system, one for the Fe-rich samples and one for the Co-rich ones, shown in figure 4. The structure observed in the Fe-rich samples (AFF phase) is characterized by ferromagnetic lines along the a (or b) direction which alternate antiferromagnetically along the transverse direction. This structure has been denominated *super-antiferromagnetic* in the context of the planar Ising model [21], and we will refer to it as SAF1. The structure appearing for Co-rich samples (both in the AFC and AFI phases) is a different kind of super-antiferromagnetic ordering, which we will call SAF2, characterized by pairs of ferromagnetic lines along the diagonal direction perpendicular to the easy axis, which alternate antiferromagnetically along the easy axis. If we make a simple balance of exchange couplings for the bonds connecting each spin to its nearest and next-nearest neighbors on the plane, we easily see that (i) nn interactions are frustrated for both structures, and (ii) nnn interactions are also frustrated in the SAF2 structure, whose energy balance amounts to zero. This structure, then, could never be stable against SAF1. However, the energy of SAF2 would not sum to zero if we allowed for two distinct nnn couplings, as implied from figure 3. Allowing for different J_2 and J_2' , respectively along the easy axis (dotted line in figure 3) and perpendicular to it, we now analyze the relative stability of the SAF1 and SAF2 structures, also in comparison to the Néel AF ordering (NAF) and the ferromagnetic (FM) state. The ground-state energy per spin in each case (leaving aside the spin value) can be written as

$$\begin{aligned} \varepsilon_{\text{SAF1}} &= 2(J_2 + J_2'), & \varepsilon_{\text{NAF}} &= 4J_1 - 2(J_2 + J_2'), \\ \varepsilon_{\text{D2SAF2}} &= 2(J_2 - J_2'), & \varepsilon_{\text{FM}} &= -4J_1 - 2(J_2 + J_2'). \end{aligned} \quad (2)$$

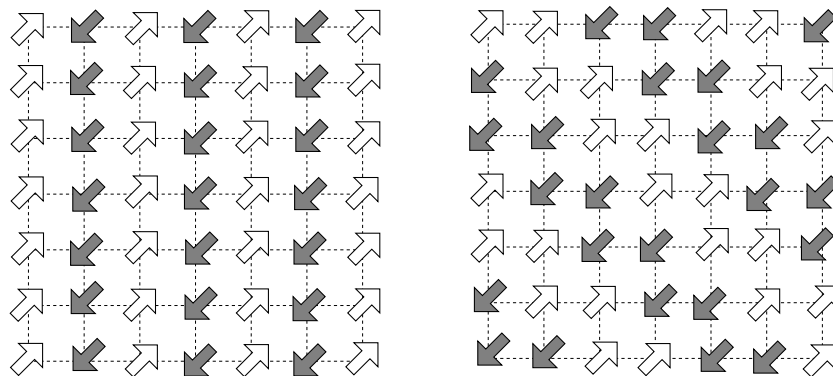


Figure 4. Spin patterns on the ab plane observed in the $(\text{Fe, Co})\text{Ta}_2\text{O}_6$ system. Left: Fe-rich samples (SAF1). Right: Co-rich samples (SAF2). For clarity, we represent opposite spins in different shades.

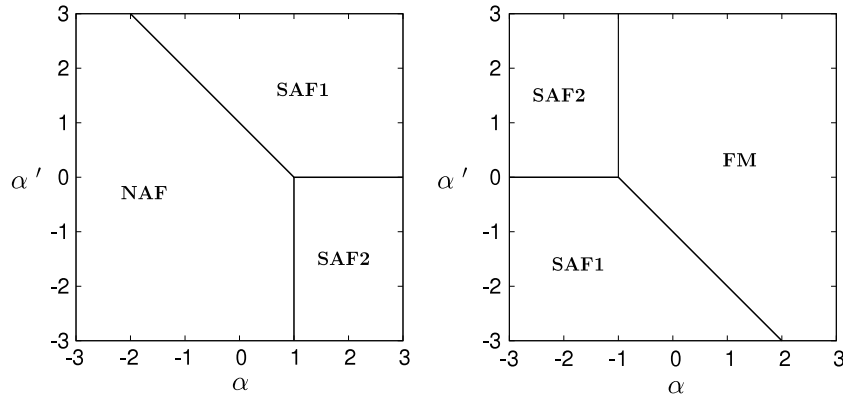


Figure 5. Phase diagrams on the α, α' plane for fixed $J_1 < 0$ (left) and $J_1 > 0$ (right).

Defining $\alpha \equiv J_2/J_1$ and $\alpha' \equiv J'_2/J_1$, we can construct the phase diagrams shown in figure 5. There we can see that the SAF2 ordering is not stable along the line $\alpha' = \alpha$. Thus, the simplified model of equation (1) cannot account for the magnetic structure observed in Co-rich samples. Nevertheless, a fitting of the susceptibility data to the corresponding high-temperature series up to order T^{-4} has been performed before [13] for the entire (Fe, Co)Ta₂O₆ series, with seemingly reasonable results, consistent with the ones originally obtained for FeTa₂O₆ [2]. The problem with such a fitting is that the number of parameters of the Hamiltonian that are being determined exceeds the number of free adjustable parameters, since we do not have access to individual components of the susceptibility tensor in the case of powder samples. With model (1) one has to determine the values of five parameters ($J_1, J_2, D, g_{\parallel}$, and g_{\perp}) from four coefficients of the high-temperature series. The result is then highly dependent on the initial values, and many different sets of parameters give comparable fittings.

We have just concluded that we need to take into account one extra parameter, J'_2 . This makes the situation even worse, since deriving terms beyond fourth order in the high-temperature series is a huge task. However, thanks to the strong easy-axis anisotropy observed for the whole series of compounds, it should be reasonable to utilize an Ising model. With this assumption, we keep only terms involving the z component of spin operators in equation (1) and drop the anisotropy term, writing the Hamiltonian as

$$\mathcal{H} = -2J_1 \sum_{\langle ij \rangle} S_i^z S_j^z - 2J_2 \sum_{\langle ij \rangle} S_i^z S_j^z - 2J'_2 \sum_{\langle ij \rangle} S_i^z S_j^z - gH_z \sum_i S_i^z, \quad (3)$$

where \parallel and \perp are relative to the anisotropy axis. Notice that by assuming an effective Ising model the only allowed values of S_i^z are $\pm S$, even though we are dealing with $S > 1/2$.

We are now left with four parameters: three exchange constants and one g -factor. Writing the susceptibility series as

$$\chi = \frac{c}{T} \left(1 + \frac{a_1}{T} + \frac{a_2}{T^2} + \frac{a_3}{T^3} + \dots \right), \quad (4)$$

we recalculated the four coefficients c, a_1, a_2 , and a_3 in terms of the parameters J_1, J_2, J'_2 , and g of equation (3). A detailed revision of high-temperature series expansions would be out of place here. We just mention the basic aspects of the method. The susceptibility is evaluated as the second derivative of the free energy with respect to the applied magnetic field in the limit where this field goes to zero. The free energy, in turn, is related to the partition function, whose expansion in powers of $1/T$ involves averages of increasingly higher powers of the Hamiltonian. These averages are evaluated at infinite temperature, i.e., with equally probable spin states. Employing this procedure with the model of equation (3), we obtain the relations listed below.

$$\begin{aligned} c &= g^2 \mu_B^2 S^2 / k_B, \\ a_1 &= 4S^2 (2J_1 + J_2 + J'_2), \\ a_2 &= 8S^4 [6J_1^2 + J_2^2 + J_2'^2 + 8J_1(J_2 + J'_2) + 4J_2 J_2'], \\ a_3 &= \frac{8}{3} S^6 [104J_1^3 + 4(J_2^3 + J_2'^3) \\ &\quad + 96J_1(J_2^2 + J_2'^2 + 6J_2 J_2') \\ &\quad + 40(J_2^2 J_2' + J_2 J_2'^2) + 198J_1^2 (J_2 + J_2')]. \end{aligned} \quad (5)$$

Equations (4) and (5) allow us to fit our susceptibility data and determine the model parameters. Actually, in the case of powder samples a factor of $1/3$ has to be included in the right-hand side of the first line in equations (5) due to averaging over the field orientations.

We want to emphasize that a careful procedure is needed to achieve trustful fittings. First, we perform a fitting to the Curie–Weiss law, $\chi = C/(T - \theta_W)$, in the range of higher temperatures, obtaining accurate values for the constants C and θ_W . These determine, respectively, the values of the coefficients c and a_1 of equation (4), which are kept fixed in the subsequent fitting procedure. Next, we adjust the formal susceptibility series typically up to order T^{-6} , enforcing the above mentioned constraints on c and a_1 . We assume an effective uniform system, with the spin S obtained by averaging the corresponding high-spin values for Fe and Co. Finally, using equations (5), we obtain the g -factor from the adjusted value of c , and the three exchange constants from the values of a_1, a_2 and a_3 . This last step involves numerically

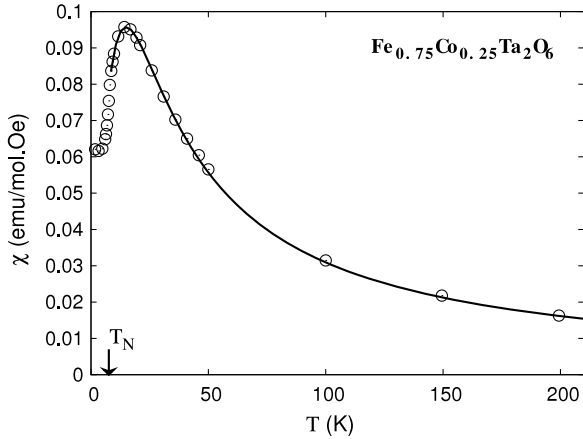


Figure 6. Susceptibility as a function of temperature for the $\text{Fe}_{0.75}\text{Co}_{0.25}\text{Ta}_2\text{O}_6$ composition. The circles are experimental points while the continuous line is the high-temperature series fitting with model (3). The Néel temperature of 7.6 K for this sample is indicated by the arrow.

solving a system of three nonlinear equations, the last three of equations (5). To illustrate the fitting results, we present typical susceptibility data together with the corresponding fitted curve in figure 6. Notice that the fitting extends down to very near the Néel temperature.

Fitted values of the exchange constants are shown in figure 7 as functions of the Fe fraction x . It can be seen that the dominant exchange interaction is J_2 , i.e., the nnn coupling along the easy axis, which is always antiferromagnetic. The other two exchange constants, J_1 and J'_2 have smaller absolute values, and change sign around the concentration $x = 0.46$, where the planar spin structure changes from SAF2 to SAF1. These results are in full agreement with the phase diagrams of figure 5. On the other hand, we can also see significant changes near the bicritical point at $x \simeq 0.01$. This may reflect the fact that a purely two-dimensional model is not enough to describe the susceptibility, since in the transition at small x involves two ordered phases that present the same in-plane magnetic structure.

Concerning the relative intensities of the various exchange couplings as well as the sign change observed for J_1 and J'_2 , it should be noticed that the latter two are related to superexchange paths that are not straight lines, in contrast to J_2 , as can be seen in figure 3. The dependence of exchange constants on bond angles was first demonstrated in the pioneering works of Goodenough [22, 23] and Kanamori [24], for direct cation–cation coupling, and for the case of one intervening anion. Here the situation is still more complex, as there are two intervening anions. In addition, the 3d- t_{2g} manifold has different fillings for Co and Fe, the orbitals tend to have different spatial extents as the ion charge changes, and the crystal-field splitting of these levels is varying with x , following the evolution of the distortion index of the oxygen octahedra [13]. Even though a microscopic analysis of the relevant superexchange processes has not yet been done, it is possible to infer from figure 3 that different orbitals are involved in the processes determining J_2 with respect to the

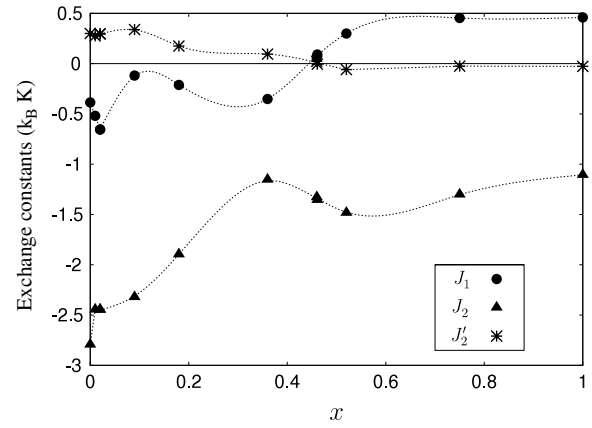


Figure 7. Exchange constants of the model Hamiltonian (3) for varying x values throughout the $\text{Fe}_x\text{Co}_{1-x}\text{Ta}_2\text{O}_6$ series, as obtained from fittings of the susceptibility data to the corresponding high-temperature series. Lines between symbols are just guides to the eye.

other two couplings, which could be the origin of the observed differences in sign and strength.

4. Conclusions

In this work, combining information obtained from neutron-diffraction and magnetic-susceptibility measurements, we complemented the T versus x magnetic phase diagram of [13] for the $\text{Fe}_x\text{Co}_{1-x}\text{Ta}_2\text{O}_6$ series. The coexistence of two distinct magnetic phases was observed around a new bicritical point located near $x = 0.01$, similarly to what had been observed around $x = 0.46$ [13]. All the low-temperature magnetic structures reflect the presence of a large magnetocrystalline anisotropy, with easy axes that alternate between the [110] and $\bar{1}\bar{1}0$ directions on neighboring magnetic planes. These directions coincide with the shortened principal axes of oxygen octahedra that surround each magnetic ion. Two in-plane patterns of magnetic moments appear, for Fe-rich and Co-rich samples, but the latter also shows two different periodicities along the c axis, yielding three distinct magnetic phases.

At high temperatures, the paramagnetic susceptibility can be described within a two-dimensional model of exchange-coupled localized spins. In contrast to what was previously done for FeTa_2O_6 [2], we introduced two different next-nearest-neighbor exchange interactions (parallel and perpendicular to the anisotropy axis). We calculated the coefficients of the high-temperature series of $\chi(T)$ up to order T^{-4} for this new model, using it to fit the paramagnetic susceptibility data. With this we were able to obtain values of the exchange constants which are consistent with the in-plane magnetic structures observed by neutron diffraction.

It is worth noticing that all the low-temperature magnetic phases present well defined periodicities both in the ab plane and along the c axis. It is thus clear that, despite the quasi-two-dimensional character of these compounds, they order in three dimensions. The complex magnetic structures observed may result from subtle changes in the intraplane and interplane couplings, within the constraints imposed by a strong magnetic

anisotropy with alternating orientations of the easy axes. While the in-plane interactions have been successfully modeled here, progress must still be made in the understanding of interplane coupling. For both of these interactions a detailed analysis of the relevant superexchange processes is also needed in order to provide microscopic justification for the model.

Acknowledgments

This work was supported in part by the French–Brazilian agreement CAPES-COFECUB and the Brazilian agency CNPq. The authors would like to thank Claudine Lacroix for interesting discussions. The financial support of the Region Rhone-Alpes (France) via the ARCUS-Brésil cooperation program is also warmly acknowledged.

References

- [1] Eicher S M, Greedan J E and Lushington K J 1986 *J. Solid State Chem.* **62** 220
- [2] Muraoka Y, Idogaki T and Uryu N 1988 *J. Phys. Soc. Japan* **57** 1758
- [3] Zawislak L I, da Cunha J B M, Vasquez A and dos Santos C A 1995 *Solid State Commun.* **94** 345
- [4] Chung E M L, Lees M R, McIntyre G J, Wilkinson C, Balakrishnan G, Hague J P, Visser D and Paul D McK 2004 *J. Phys.: Condens. Matter* **16** 7837
- [5] Hague J P, Chung E M L, Visser D, Balakrishnan G, Clementyev E, Paul D McK and Lees M R 2005 *J. Phys.: Condens. Matter* **17** 7227
- [6] Kremer R K, Greedan J E, Gmelin E, Dai W, White M A, Eicher S M and Lushington K J 1988 *J. Physique* **49** 1495
- [7] Ehrenberg H, Wltschek G, Rodriguez-Carvajal J and Vogt T 1988 *J. Magn. Magn. Mater.* **184** 111
- [8] Reimers J N, Greedan J E, Stager C V and Kremer R K 1989 *J. Solid State Chem.* **83** 20
- [9] Borromei R, Cavallie E and Oleari L 1993 *Inorg. Chim. Acta* **204** 159
- [10] Kremer R K and Greedan J E 1988 *J. Solid State Chem.* **73** 579
- [11] Kinast E J, dos Santos C A, Schmitt D, Isnard O, Gusmão M A and da Cunha J B M 2010 *J. Alloys Compounds* **491** 41
- [12] Ye J H, Matsushita A and Zou Z G 2003 *Int. J. Hydrogen Energy* **28** 651
- [13] Kinast E J, Antonietti V, Schmitt D, Isnard O, da Cunha J B M, Gusmão M A and dos Santos C A 2003 *Phys. Rev. Lett.* **91** 197208
- [14] de Oliveira Neto S R, Kinast E J, Gusmão M A, dos Santos C A, Isnard O and da Cunha J B M 2007 *J. Phys.: Condens. Matter* **19** 356210
- [15] Oliveira Neto S R, Kinast E J, Isnard O, da Cunha J B M, Gusmão M A and dos Santos C A 2008 *J. Magn. Magn. Mater.* **320** e125
- [16] Antonietti V, Kinast E J, Zawislak L I, da Cunha J B M and dos Santos C A 2001 *J. Phys. Chem. Solids* **62** 1239
- [17] Arrott A 1957 *Phys. Rev.* **108** 1394
- [18] Rodriguez-Carvajal J 1993 *Physica B* **192** 55
- [19] McCusker L B, Von Dreele R B, Cox D E, Louer D and Scardi P 1999 *J. Appl. Crystallogr.* **32** 36
- [20] Sears V F 1992 *Neutron News* **3** 26
- [21] Fan C and Wu F Y 1969 *Phys. Rev.* **179** 560
- [22] Goodenough J B 1958 *J. Phys. Chem. Solids* **6** 287
- [23] Goodenough J B 1963 *Magnetism and the Chemical Bond* (New York: Interscience)
- [24] Kanamori J 1959 *J. Phys. Chem. Solids* **10** 87